10. WHO. Global surveillance, diagnosis and therapy of human transmissible spongiform encephalopathies: report of a WHO consultation. *World Health Organization: Emerging and Other Communicable Diseases, Surveillance and Control.* Geneva: WHO, 1998.
11. Satoh K, Tobiume M, Matsui Y, *et al.* Establishment of a standard 14-3-3 protein assay of cerebrospinal fluid as a diagnostic tool for Creutzfeldt–Jakob disease. *Lab Invest* 2010;90:1637–44.
12. Kitamoto T, Shin RW, Doh-ura K, *et al.* Abnormal isoform of prion proteins accumulates in the synaptic structures of the central nervous system in patients with Creutzfeldt–Jakob disease. *Am J Pathol* 1992;140:1285–94.
13. Kitamoto T, Ohata M, Doh-ura K, *et al.* Novel missense variants of prion protein in Creutzfeldt–Jakob disease or Gerstmann-Sträussler syndrome. *Biochem Biophys Res Commun* 1993;191:709–14.
14. Shimizu S, Hoshi K, Muramoto T, *et al.* Creutzfeldt–Jakob disease with florid-type plaques after cadaveric dura mater grafting. *Arch Neurol* 1999;56:357–62.
15. Satoh K, Shirabe S, Eguchi H, *et al.* 14-3-3 protein, total tau and phosphorylated tau in cerebrospinal fluid of patients with Creutzfeldt–Jakob disease and neurodegenerative disease in Japan. *Cell Mol Neurobiol* 2006;26:45–52.
16. Atarashi R, Satoh K, Sano K, *et al.* Ultrasensitive human prion detection in cerebrospinal fluid by real-time quaking-induced conversion. *Nat Med* 2011;17:175–8.
17. Hirai T, Korogi Y, Arimura H, *et al.* Intracranial aneurysms at MR angiography: effect of computer-aided diagnosis on radiologists' detection performance. *Radiology* 2005;237:605–10.
18. Kallenberg K, Schulz-Schaeffer WJ, Jastrow U, *et al.* Creutzfeldt–Jakob disease: comparative analysis of MR imaging sequences. *AJNR Am J Neuroradiol* 2006;27:1459–62.
19. Murata T, Shiga Y, Higano S, *et al.* Conspicuity and evolution of lesions in Creutzfeldt–Jakob disease at diffusion-weighted imaging. *AJNR Am J Neuroradiol* 2002;23:1164–72.
20. Parchi P, Giese A, Capellari S, *et al.* Classification of sporadic Creutzfeldt–Jakob disease based on molecular and phenotypic analysis of 300 subjects. *Ann Neurol* 1999;46:224–33.
21. Meissner B, Kallenberg K, Sanchez-Juan P, *et al.* MRI lesion profiles in sporadic Creutzfeldt–Jakob disease. *Neurology* 2009;72:1994–2001.
22. Diagnostic criteria for sporadic CJD from 1 January 2010. *National Creutzfeldt–Jakob Disease Surveillance Diagnostic Criteria [online].* http://www.cjd.ed.ac.uk/criteria.htm (accessed 3 Oct 2011).
23. Young GS, Geschwind MD, Fischbein NJ, *et al.* Diffusion-weighted and fluid-attenuated inversion recovery imaging in Creutzfeldt–Jakob disease: high sensitivity and specificity for diagnosis. *AJNR Am J Neuroradiol* 2005;26:1551–62.
24. Lin YR, Young GS, Chen NK, *et al.* Creutzfeldt–Jakob disease involvement of rolandic cortex: a quantitative apparent diffusion coefficient evaluation. *AJNR Am J Neuroradiol* 2006;27:1755–9.
25. Fujita K, Nakane S, Harada M, *et al.* Diffusion tensor imaging in patients with Creutzfeldt–Jakob disease. *J Neurol Neurosurg Psychiatry* 2008;79:1304–6.
26. Hamaguchi T, Kitamoto T, Sato T, *et al.* Clinical diagnosis of MM2-type sporadic Creutzfeldt–Jakob disease. *Neurology* 2005;64:643–8.

J Neuropathol Exp Neurol

Vol. 71, No. 8
August 2012
pp. 750–759

ORIGINAL ARTICLE

Characteristics of Aquaporin Expression Surrounding Senile Plaques and Cerebral Amyloid Angiopathy in Alzheimer Disease

Akihiko Hoshi, MD, PhD, Teiji Yamamoto, MD, PhD, Keiko Shimizu, MT, Yoshikazu Ugawa, MD, PhD, Masatoyo Nishizawa, MD, PhD, Hitoshi Takahashi, MD, PhD, and Akiyoshi Kakita, MD, PhD

Abstract

Senile plaques (SPs) containing amyloid β peptide (Aβ) 1–42 are the major species present in Alzheimer disease (AD), whereas Aβ1–40 is the major constituent of arteriolar walls affected by cerebral amyloid angiopathy. The water channel proteins astrocytic aquaporin 1 (AQP1) and aquaporin 4 (AQP4) are known to be abnormally expressed in AD brains, but the expression of AQPs surrounding SPs and cerebral amyloid angiopathy has not been described in detail. Here, we investigated whether AQP expression is associated with each species of Aβ deposited in human brains affected by either sporadic or familial AD. Immunohistochemical analysis demonstrated more numerous AQP1-positive reactive astrocytes in the AD cerebral cortex than in controls, located close to Aβ42- or Aβ40-positive SPs. In AD cases, however, AQP1-positive astrocytes were not often observed in Aβ-rich areas, and there was a significant negative correlation between the levels of AQP1 and Aβ42 assessed semiquantitatively. We also found that Aβ plaque-like AQP4 was distributed in association with Aβ42- or Aβ40-positive SPs and that the degree of AQP4 expression around Aβ40-positive vessels was variable. These findings suggest that a defined population of AQP1-positive reactive astrocytes may modify Aβ deposition in the AD brain, whereas the Aβ deposition process might alter astrocytic expression of AQP4.

Key Words: Amyloid-β peptides 42 and 40, Aquaporin 1, Aquaporin 4, Alzheimer disease, Cerebral amyloid angiopathy, Senile plaques.

INTRODUCTION

Alzheimer disease (AD) is characterized pathologically by abnormal accumulation of extracellular aggregates of amyloid-β peptide (Aβ) in the form of senile plaques (SPs) (1). A major component of these SPs is Aβ 1–42 (Aβ42), and the presence of Aβ 1–40 (Aβ40)–positive amyloid seems to be related to the development of SPs (2). Although they differ in only 2 amino acid residues at the C-terminal end, Aβ42 shows a stronger tendency to aggregate and is more toxic to neurons than Aβ40 (3). On the other hand, the major vascular pathology in AD is cerebral amyloid angiopathy (CAA), which results from Aβ40 deposition in arteriolar media (1, 4). Proportions of vessels containing Aβ40 deposits varied considerably among AD cases, and the severity of AD is not correlated with the extent of parenchymal Aβ deposition (1, 5). Despite extensive studies, how SPs and CAA are formed or degraded and how they relate to AD pathogenesis are still unclear.

The role of astroglia in Aβ processing and metabolism also remains unclear, but reactive astrocytosis in AD suggests their participation in the clearance and degradation of Aβ (6–9). Indeed, reactive astrocytes often surround SPs or CAA in AD brains; thus, they seem to regulate Aβ deposition (10, 11). Several recent studies have demonstrated that some of the water channel proteins, astrocytic aquaporin 1 (AQP1) and/or aquaporin 4 (AQP4), are abnormally expressed in AD brains (12–15). AQP1 is normally expressed in the apical membrane of the choroid plexus and participates in the formation of cerebrospinal fluid (16–19). AQP4 shows polarized localization in astrocyte foot processes where it is involved in brain edema formation in cases of stroke, brain tumor, acute bacterial meningitis, and brain abscess (18–23).

Differences between astrocytic AQP1 and AQP4 expression around SPs and CAA have not been investigated in detail. Thus, the precise roles of AQP expression in AD remain unknown. Because these channels are often localized near sites of Aβ deposition, we hypothesized that they might play a pivotal role in the degenerative processes of AD by modifying Aβ pathology. Therefore, we investigated whether AQP1 or AQP4 expression was associated with deposition of each Aβ species in human brains with advanced AD.

MATERIALS AND METHODS

Neuropathologic Assessment

Informed consent for research on all brain tissue was obtained from the Brain Research Institute, University of Niigata. The study was approved by the Ethics Committee of Fukushima Medical University. Autopsied brains of 8 patients with AD (5 with sporadic AD [sAD] and 3 with familial AD [fAD]) were examined and compared with the brains of 5 age-matched controls experiencing nonneurologic conditions. Each diagnosis was based on both clinical history and postmortem neuropathologic verification (24). Clinical data for the 13 patients are summarized in the Table. In all cases, the temporal lobes (superior, middle, and inferior temporal gyrus)

From the Department of Neurology (AH, TY, KS, YU), Fukushima Medical University, Fukushima; Departments of Neurology (MN) and Pathology (HT, AK), Brain Research Institute, University of Niigata, Niigata, Japan.
Send correspondence and reprint requests to: Akihiko Hoshi, MD, PhD, Department of Neurology, Fukushima Medical University, Fukushima 960-1295, Japan; E-mail: hoshia@fmu.ac.jp
This work was supported by a Collaborative Research Project Grant (2224) from the Brain Research Institute, University of Niigata, Niigata, Japan.
Supplemental digital content is available for this article. Direct URL citations appear in the printed text and are provided in the HTML and PDF versions of this article on the journal's Web site (www.jneuropath.com).

TABLE. Patient Clinical and Neuropathologic Data

Case	Sex	Age at Death, y	PMI, h	Braak Stage	Brain Weight, g	Aβ42 Deposit	Aβ40 Deposits
Control 1	M	76	3.5		1,270	1	0
Control 2	M	80	3		1,300	1–2	1
Control 3	F	82	4.5		1,210	1	1
Control 4	M	77	22		1,175	1–2	1
Control 5	M	76	2		1,275	1	0
sAD1	F	104	3.5	VI/C	780	3–4	2–3
sAD2	F	86	4.5	VI/C	860	3–4	1
sAD3	F	86	4	VI/C	995	4	2–3
sAD4	F	100	3	VI/C	935	3	1
sAD5	M	78	3.5	VI/C	910	3–4	1–2
fAD1	F	65	3.5	VI/C	750	4	1
fAD2	F	57	4	VI/C	470	4	2–3
fAD3	F	66	3	VI/C	910	4	1

Grading of Aβ 42 and 40 deposits: 0 = absent, 1 = few, 2 = moderate, 3 = many, 4 = very many.
sAD indicates sporadic Alzheimer disease; fAD, familial Alzheimer disease; fAD mutations: fAD1, fAD3, amyloid precursor protein (APP), 717Vallle; fAD2, presenilin L381V. M, male; F, female; PMI, postmortem interval.

were used for the immunohistochemical study. The extent of Aβ42 and Aβ40 deposition in immunostained sections was rated semiquantitatively, as previously reported (4).

Immunohistochemistry

Tissue samples were processed into 4-μm-thick paraffin-embedded sections, and immunostaining was performed using the EnVision (Dako, Glostrup, Denmark) system. The sections were deparaffinized, and nonspecific binding was blocked with 2.4% goat serum and 30% H_2O_2 for 30 minutes at room temperature. After washing with phosphate-buffered saline, the slides were incubated overnight at 4°C with primary antibodies. The primary antibodies and dilutions used were rabbit polyclonal anti-AQP1 antibody (1:1000; Chemicon International, Temecula, CA), rabbit polyclonal anti-AQP4 antibody (1:500; Santa Cruz Biotechnology, Santa Cruz, CA), rabbit polyclonal anti-Aβ42 antibody (1:500; Calbiochem, Billerica, MA), rabbit polyclonal anti-Aβ40 antibody (1:500; Calbiochem, Millipore), and mouse monoclonal anti–glial fibrillary acidic protein (GFAP) antibody (1:1000; Chemicon). For Aβ40 or Aβ42 immunostaining, sections were pretreated with 98% formic acid for 5 minutes. Subsequently, secondary antibody incubations were carried out for 45 minutes at room temperature. Peroxidase labeling was visualized using diaminobenzidine as a chromogen. For double staining, we used the EnVision G|2 double-stain system (Dako) in accordance with the manufacturer's protocol. Visualization was based on peroxidase using diaminobenzidine and alkaline phosphatase with permanent red as the chromogen.

Fluorescence immunohistochemistry was also performed on paraffin sections to characterize the relationship between the expression of AQP and that of Aβ. The primary antibodies and dilutions used were rabbit polyclonal anti-AQP1 antibody (1:1000), mouse monoclonal anti-Aβ42 antibody (1:300; Millipore), rabbit polyclonal anti-AQP4 antibody (1:500), and mouse monoclonal anti-Aβ40 antibody (1:25; Immuno-Biological Laboratories Co., Gunma, Japan). The secondary antibodies and dilutions used were fluorescein isothiocyanate–coupled goat anti-mouse IgG (1:100; KPL, Gaithersburg, MD), and Cy3-conjugated donkey anti-rabbit IgG (1:100; Jackson ImmunoResearch, West Grove, PA). Immunostained sections and fluorescent specimens were analyzed using a microscope digital camera system (DP70; Olympus, Tokyo, Japan).

Statistical Analysis

In all AD cases, the fluorescence intensity of AQP1 and Aβ42 was evaluated as relative fluorescence units and quantified using image analysis software (Lumina Vision; Mitani Corp., Tokyo, Japan), as reported previously (21). About 4 to 6 areas of 0.14 mm^2 were randomly selected from photographs of specimens that had been immunostained for AQP1 and Aβ42 taken from the superior, middle, and inferior temporal cortices of patients with AD. Correlations between AQP1 and Aβ42 levels in relative fluorescence units were assessed using both Spearman correlation and regression analyses. Statistical significance was set at $p < 0.05$. AQP1 or AQP4 immunoreactivity (IR) in the cerebral cortex was also semiquantified using image analysis software (Win Roof; Mitani Corp.), as described previously (25). The quantification measure, referred to as the relative density, was defined as the saturation value of AQP1 or AQP4 immunostaining on digitized images. Three random areas, each measuring 3.44 mm^2 in the superior, middle, and inferior temporal cortices, were assessed in all cases. All data were expressed as means ± SD. One-way ANOVA, followed by the Bonferroni test, was performed for statistical comparisons of the semiquantitatively measured AQP4 IR levels. Differences at $p < 0.05$ were regarded as statistically significant.

RESULTS

Aβ Deposition

All AD cases had numerous Aβ42 deposits in the cortex but the extent of Aβ40 accumulation relative to Aβ42 was highly variable (Table). Aβ40 deposits in both leptomeningeal and intracortical small vessels and capillaries were also

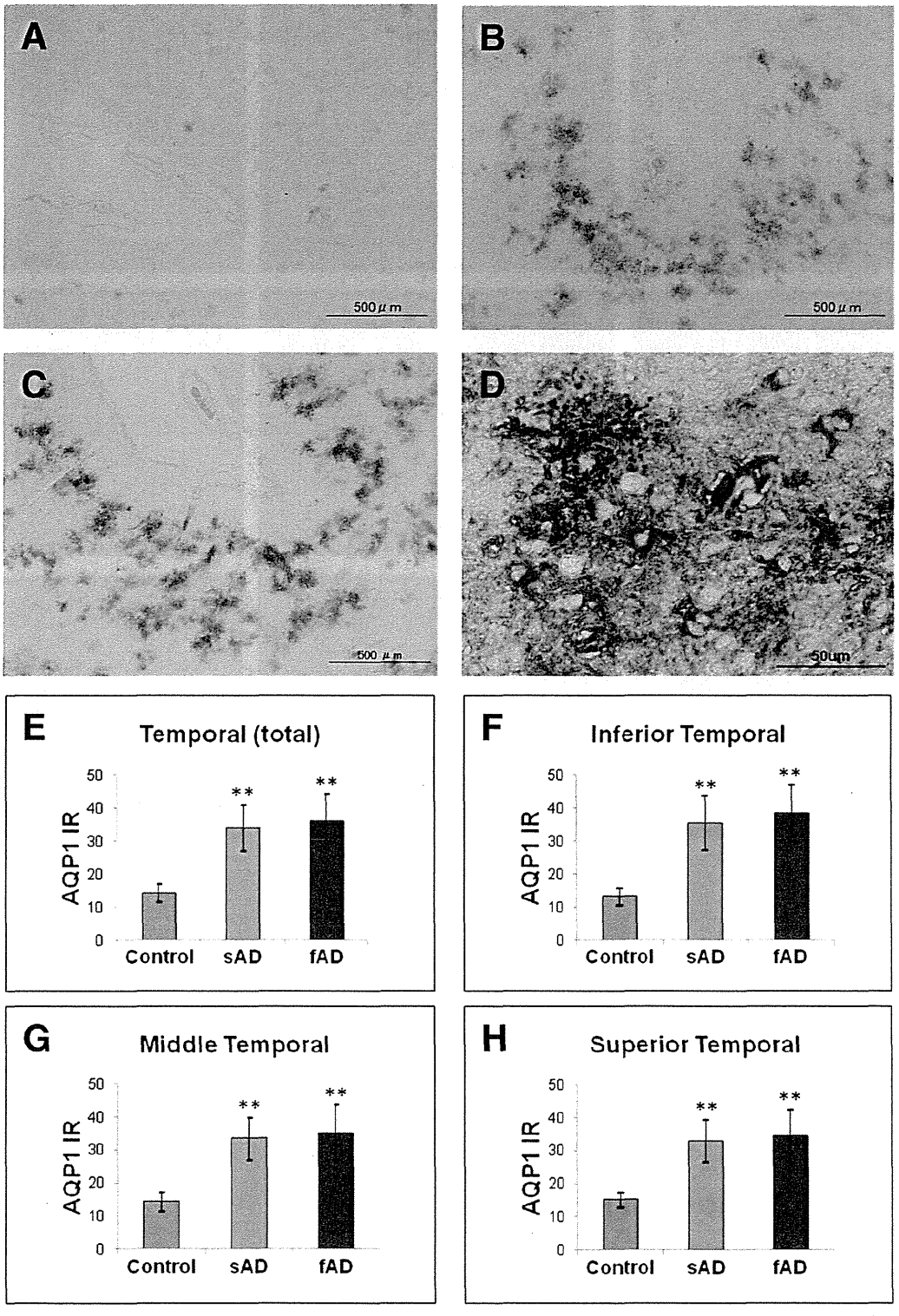

FIGURE 1. (A–D) Immunohistochemistry for aquaporin 1 (AQP1) in control brain **(A)**, and brains with sporadic Alzheimer disease (sAD) **(B)**, and familial Alzheimer disease (fAD) **(C)**. There are more numerous AQP1-positive cells in the cerebral cortex of both the sAD and fAD brains versus the controls. **(D)** Double immunolabeling of AQP1 (brown) and glial fibrillary acidic protein (GFAP) (red) in a case of AD. **(E–H)** The cortical levels of AQP1 immunoreactivity in both the sAD and fAD groups were significantly higher than in the control group. Data are given as mean ± SD. **, $p < 0.01$ versus control.

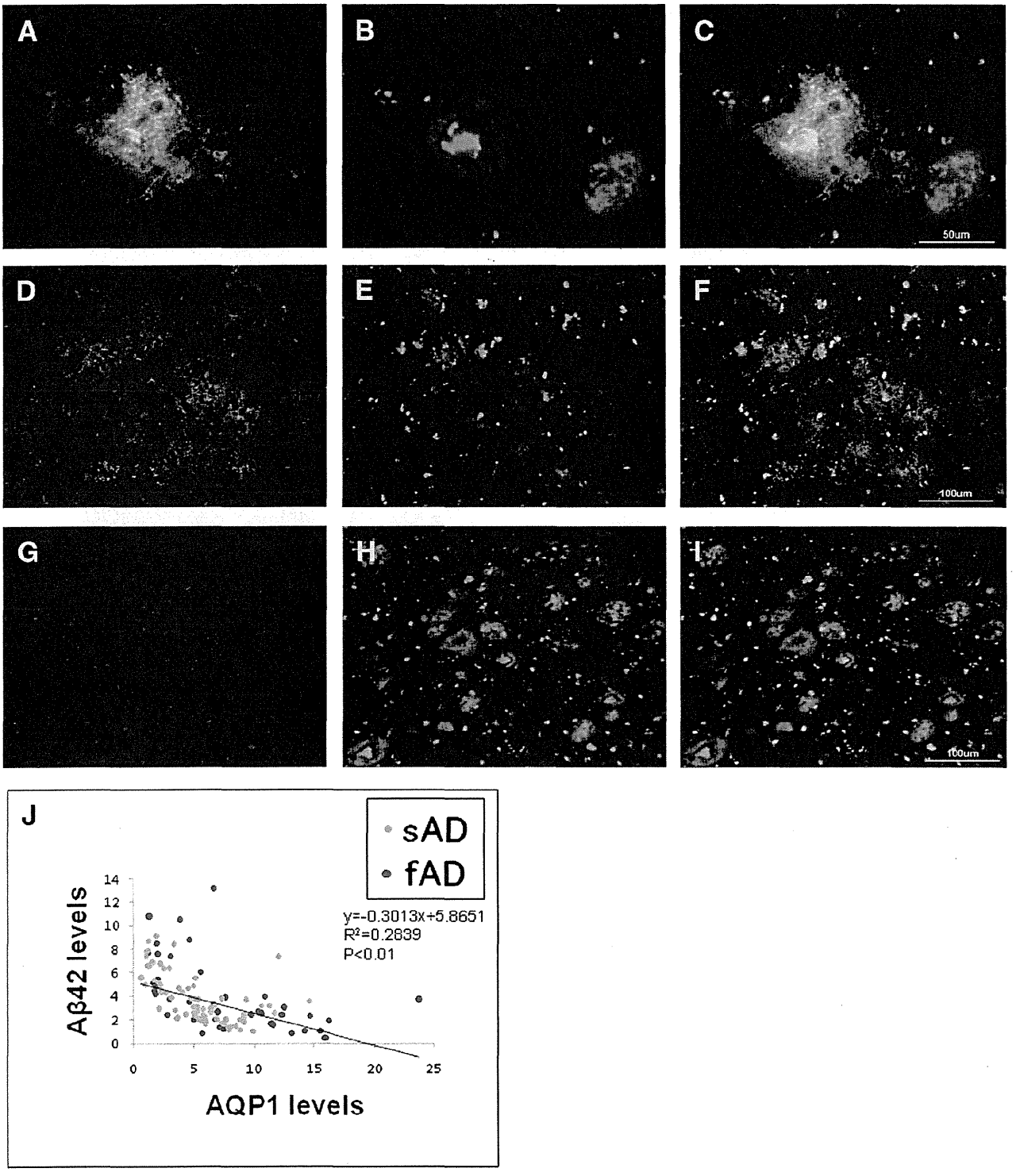

FIGURE 2. (A–I) Double immunofluorescence for aquaporin 1 (AQP1) **(A, D, G)** and amyloid-β peptide 1–42 (Aβ42) **(B, E, H)** in the Alzheimer disease (AD) groups **(C, F, I**: merged images**)**. Cells showing intense AQP1 expression are in contact with classic Aβ42 plaques **(A–C)**. Numerous AQP1-positive cells are present in areas where Aβ42 plaques are sparse **(D–F)**, but are not often observed in areas where such plaques are dense **(G–I)**. **(J)** Plot of Aβ42 levels and AQP1 levels (in relative fluorescence units) in the sporadic and familial AD groups. Semiquantitative analysis of AQP1/Aβ42 levels in both AD groups revealed a significant negative correlation between the cortical levels of AQP1 and that of Aβ42 ($R^2 = 0.2839$, $p < 0.01$).

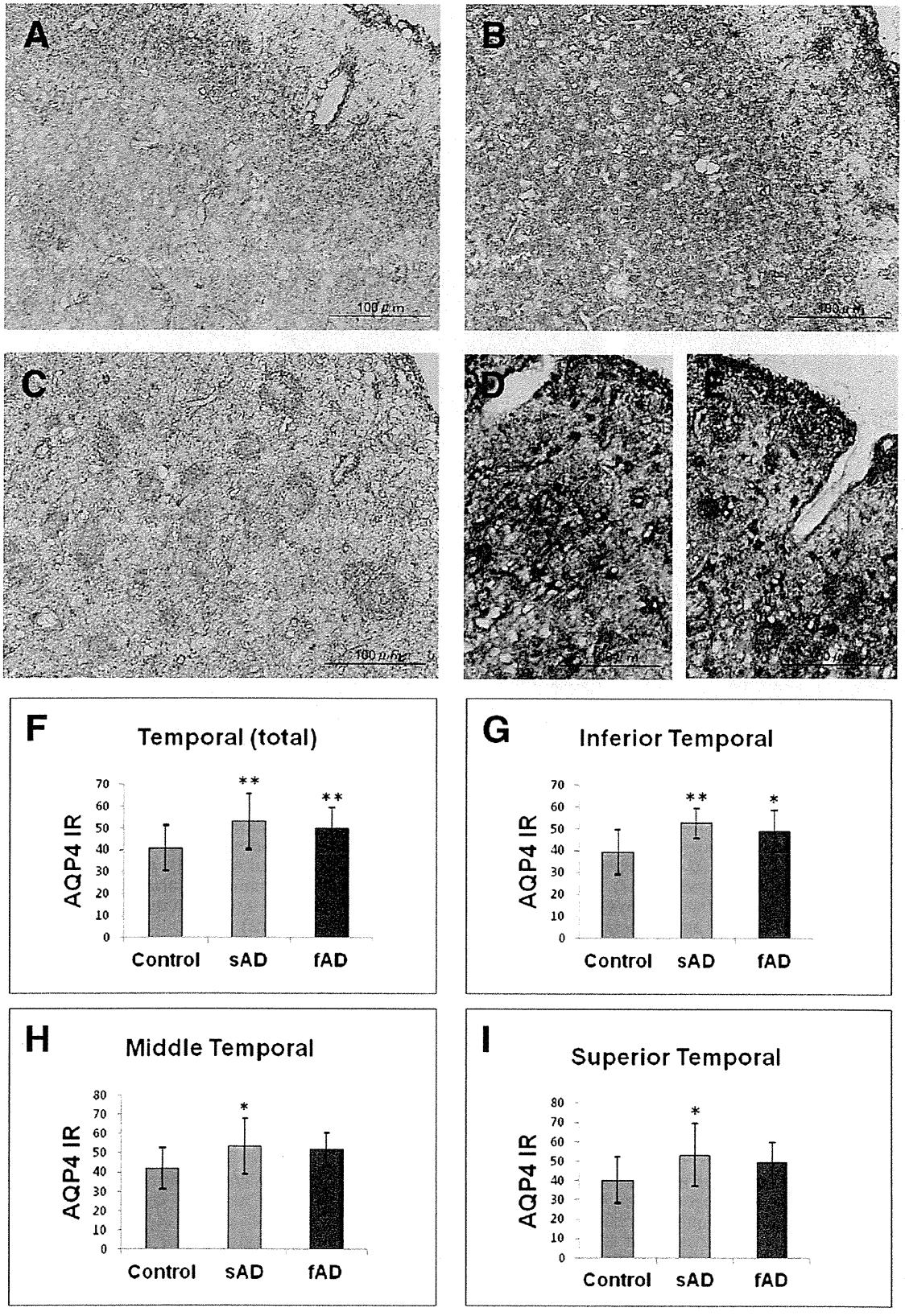

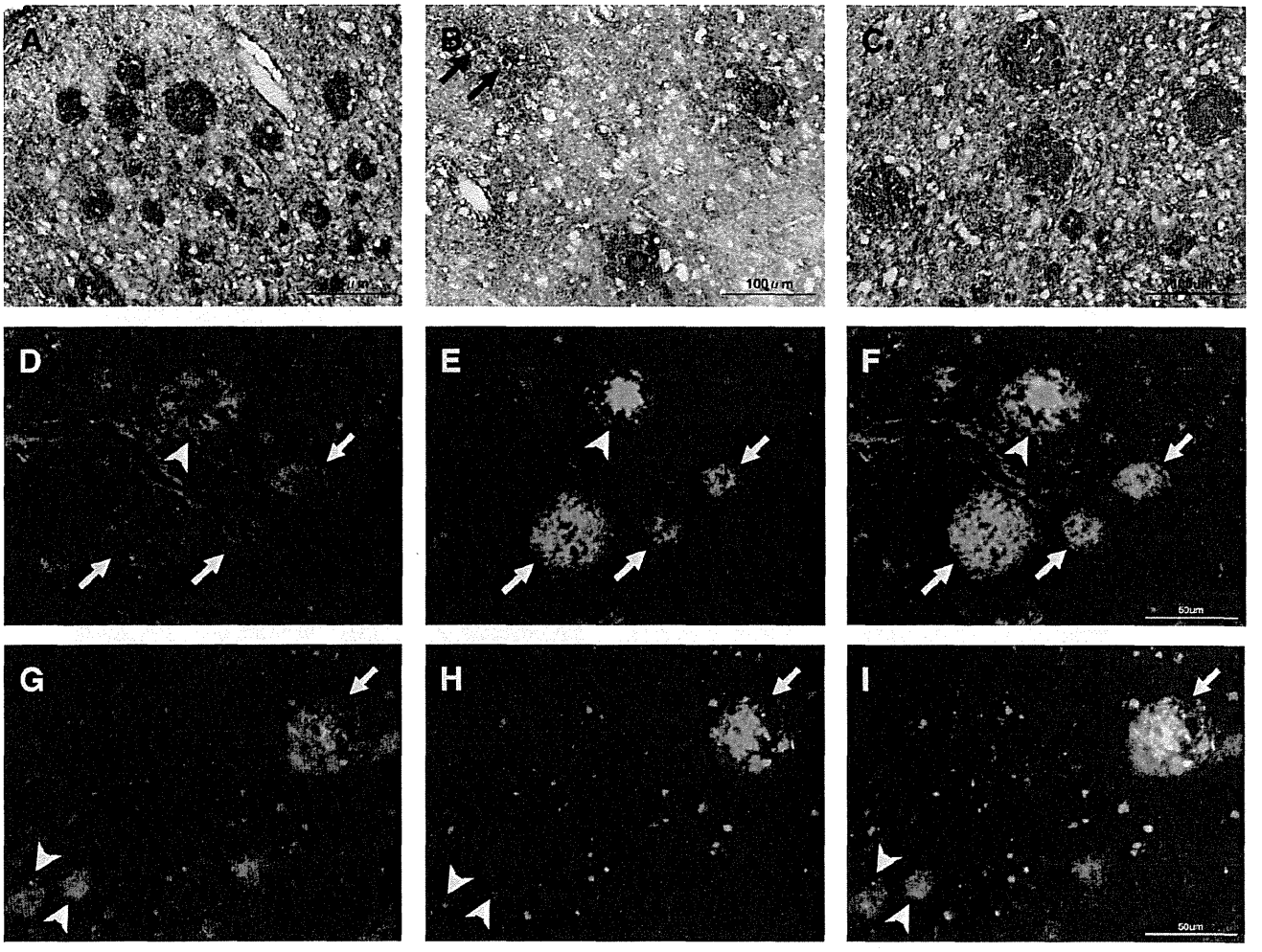

FIGURE 4. (A–C) Double-labeling immunohistochemistry for aquaporin 4 (AQP4) (brown) and amyloid-β peptide 1–42 (Aβ42) (red) **(A)** or amyloid-β peptide 1–40 (Aβ40) Aβ40 (red) **(B, C)** in cases of Alzheimer disease (AD). Numerous Aβ42 or Aβ40 plaques colocalize with intense Aβ plaque-like AQP4 expression **(A, C)**. There are smaller Aβ40-positive deposits within areas of plaque-like AQP4 expression **(B**, arrows**)**. **(D–I)** Double immunofluorescence for AQP4 **(D, G)** and Aβ42 **(E)** or Aβ40 **(H)** in the AD groups **(F, I**: AQP1/Aβ42 or Aβ40 merged images**)**. Classic Aβ42 plaques are devoid of AQP4 immunoreactivity in the dense core but show enhanced AQP4 expression at the margins **(D–F**, arrowheads**)**. AQP4 immunoreactivity is strong in the interior of primitive Aβ42 or Aβ40 plaques **(D–I**, arrows**)** or around areas of smaller Aβ40 deposits **(G–I**, arrowheads**)**.

observed in the patients with AD. Age-matched controls showed only a few or modest accumulations of Aβ42 deposits and no or only slight Aβ40 deposits (Table).

AQP1 Expression and Its Relationship to Aβ Deposition

AQP1-positive cells were more abundant in the cerebral cortex of both the sAD and fAD groups versus the controls (Figs. 1A–C). Numerous AQP1-positive cells in both AD groups were mainly in the pyramidal cell layers and had the morphologic characteristics of bushy reactive astrocytes, with hypertrophic cell bodies and highly branched processes. Double immunostaining for AQP1 and GFAP showed that these cells coexpressed both molecules (Fig. 1D). The levels of cortical AQP1 IR in both the sAD and fAD groups were significantly greater than in the control group. AQP1 IR in

FIGURE 3. (A–C) Immunohistochemistry for aquaporin 4 (AQP4) in a control brain **(A)**, and in cases of sporadic Alzheimer disease (sAD) **(B)**, and familial Alzheimer disease (fAD) **(C)**. High-power views show subpial or superficial cortical AQP4 immunostaining. **(D, E)** Double-labeling immunohistochemistry for AQP4 (brown) and glial fibrillary acidic protein (GFAP) (red) in the cortex of AD brains. AD brains showed intense AQP4 expression and GFAP-immunoreactive astrocytes **(D)** or marked Aβ plaque-like AQP4 expression **(E)**. **(F–I)** Cortical levels of AQP4 immunoreactivity in both the sAD and fAD groups are significantly greater than the in the control group, except for the middle and superior temporal cortices in the fAD group. Data are given as mean ± SD. **, $p < 0.01$ versus control; *, $p < 0.05$ versus control.

each case, expressed as the mean ± SD for the total, inferior, middle, and superior temporal cortices, was 14.2 ± 2.8, 13.2 ± 2.6, 14.2 ± 3.0, and 15.2 ± 2.4 in the control group; 34.0 ± 7.0, 35.4 ± 8.3, 33.5 ± 6.4, and 33.0 ± 6.5 in the sAD group; and 36.0 ± 8.4, 38.4 ± 8.7, 35.0 ± 8.71, and 34.5 ± 8.1 in the fAD group, respectively (Figs. 1E–H).

To confirm the observed relationship between the patterns of AQP1 and Aβ42 expression in AD, we next conducted a double immunofluorescence analysis of AQP1 and Aβ42 in all of the AD cases. AQP1-expressing cells were often localized near Aβ42 plaques in the sAD and fAD cases (Figs. 2A–F), but AQP1-positive astrocytes were not often observed in areas of densely packed Aβ42 plaques (Figs. 2G–I). There were numerous AQP1-positive cells in areas where Aβ42 plaques were sparse (Figs. 2D–F). There were significant negative correlations between the levels of AQP1 and Aβ42 expression when assessed semiquantitatively in the AD groups (Fig. 2J). Similarly, increased AQP1 IR was observed in areas where Aβ40 plaques were sparse (Figure, Supplemental Digital Content 1, Parts A and B, http://links.lww.com/NEN/A361), whereas expression was decreased in Aβ40-rich areas (Figure, Supplemental Digital Content 1, Parts C and D, http://links.lww.com/NEN/A361). In general, most AQP1-expressing cells were near Aβ40 plaques (Figure, Supplemental Digital Content 1, Parts E–G, http://links.lww.com/NEN/A361). Negative controls, in which incubation with anti-AQP1 antibody had been omitted, showed no IR (data not shown). The epithelial cells of the choroid plexus were intensely labeled with anti-AQP1 antibody (data not shown).

AQP4 Expression and Its Relationship to Aβ Deposition

Cortical AQP4 immunoreactivity was also more intense in both the sAD and fAD groups than in the control group (Figs. 3A–C; Figure, Supplemental Digital Content 2, Parts A–C, http://links.lww.com/NEN/A362). There were 2 prominent patterns of subpial or superficial cortical AQP4 immunoreactivity in the AD groups: intense diffuse AQP4 labeling of the entire neuropil (Fig. 3B) and AQP4 distribution around Aβ plaque-like bodies (Fig. 3C). The latter pattern was more apparent in fAD cases with an amyloid precursor protein mutation than in a case with a presenilin mutation (Table), but this was also seen in some patients with sAD. In the deeper cortical layers of control brains, there was less intense AQP4 immunoreactivity in cells with astrocyte morphology around vessels (Figure, Supplemental Digital Content 2, Part D, http://links.lww.com/NEN/A362). In the AD brains, intense AQP4 expression patterns that resembled astrocytic profiles (Figure, Supplemental Digital Content 2, Part E, http://links.lww.com/NEN/A362) or Aβ plaque-like AQP4 expression (Figure, Supplemental Digital Content 2, Part F, http://links.lww.com/NEN/A362) were observed in the deeper cortical layers. As shown in Figure 3, F to I, the cortical AQP4 IR in both the sAD and fAD groups was significantly greater than that in the control group, except for in the middle and superior temporal cortices in the fAD group. AQP4 IR in each case, expressed as the mean ± SD for the total, inferior, middle, and superior temporal cortices, was 40.9 ± 10.3, 39.3 ± 10.3, 41.7 ± 10.6, and 40.2 ± 12.0 in the control group; 53.1 ± 12.7, 52.6 ± 6.8, 53.4 ± 14.1, and 53.3 ± 16.3 in the sAD group; and 49.9 ± 9.2, 48.9 ± 9.2, 51.7 ± 8.9, and 49.3 ± 10.4 in the fAD group. Double labeling using both anti-AQP4 and anti-GFAP antibodies clearly showed that areas of AQP4 expression coincided with areas of GFAP expression in the cortex of the control group (data not shown). In contrast, AQP4 immunoreactivity was clearly observed in both astrocytosis and Aβ plaque-like structures in the AD groups (Figs. 3D, E).

We then conducted double-labeling immunohistochemistry for AQP4 and Aβ42 or Aβ40 in the AD cases. As expected, numerous Aβ42 or Aβ40 plaques were colocalized with intense expression of Aβ plaque-like AQP4 (Figs. 4A–C), and small Aβ40-positive deposits were detected within some areas of Aβ plaque-like AQP4 expression (Fig. 4B). To examine the expression patterns of AQP4 in both Aβ42 and Aβ40 plaques in detail, we conducted a double-immunofluorescence study of AQP4 and Aβ42 or Aβ40 in the AD groups. A noteworthy finding was that classic Aβ42 plaques were devoid of AQP4 immunoreactivity in the dense core, although AQP4 expression was enhanced at the marginal rim (Figs. 4D–F, arrowheads). Primitive Aβ42 or Aβ40 plaques showed strong AQP4 immunoreactivity in the interior (Figs. 4D–I, arrows) or around areas of light Aβ deposition (Figs. 4G–I, arrowheads).

Lastly, we investigated the expression of AQP4 around Aβ40-positive vessels, that is, larger vessels and capillaries with CAA. Intriguingly, various degrees of AQP4 expression were noted around Aβ40-positive vessels (Figs. 5B–F). Intense AQP4 immunoreactivity was observed around larger vessels showing slight to moderate Aβ40 positivity (Figs. 5B, C) in comparison to that around Aβ40-negative vessels (Fig. 5A). Loose AQP4 reaction products with irregular perivascular spaces distributed around larger vessels with intense Aβ40 positivity were also observed, in contrast to Aβ40 plaques associated with massively enhanced AQP4 expression (Fig. 5D). In addition, AQP4 expression around capillaries with CAA tended to be more intense with dyshoric changes, that is, Aβ40 spreading into the neuropil (Figs. 5E, F).

DISCUSSION

The marked variation of AQP expression in AD brains observed in the present study raises the possibility that AQP1-positive reactive astrocytes may pathologically modify the deposition of Aβ and that Aβ deposits may alter the astrocytic expression of AQP4 during the development of AD. In both the sAD and fAD groups, many AQP1-positive reactive astrocytes were close to deposits of Aβ42 or Aβ40, whereas AQP1 immunoreactivity in astrocytes was often reduced in areas of intense Aβ immunoreactivity, suggesting that AQP1 expression is associated with transition to an Aβ42- or Aβ40-rich state. Other noteworthy features included the presence of intense Aβ plaque-like AQP4 expression associated with Aβ42- or Aβ40-positive SPs and various degrees of AQP4 expression around Aβ40-positive vessels. There were no apparent differences in AQP1 expression between the sAD and fAD groups, although fAD cases with amyloid

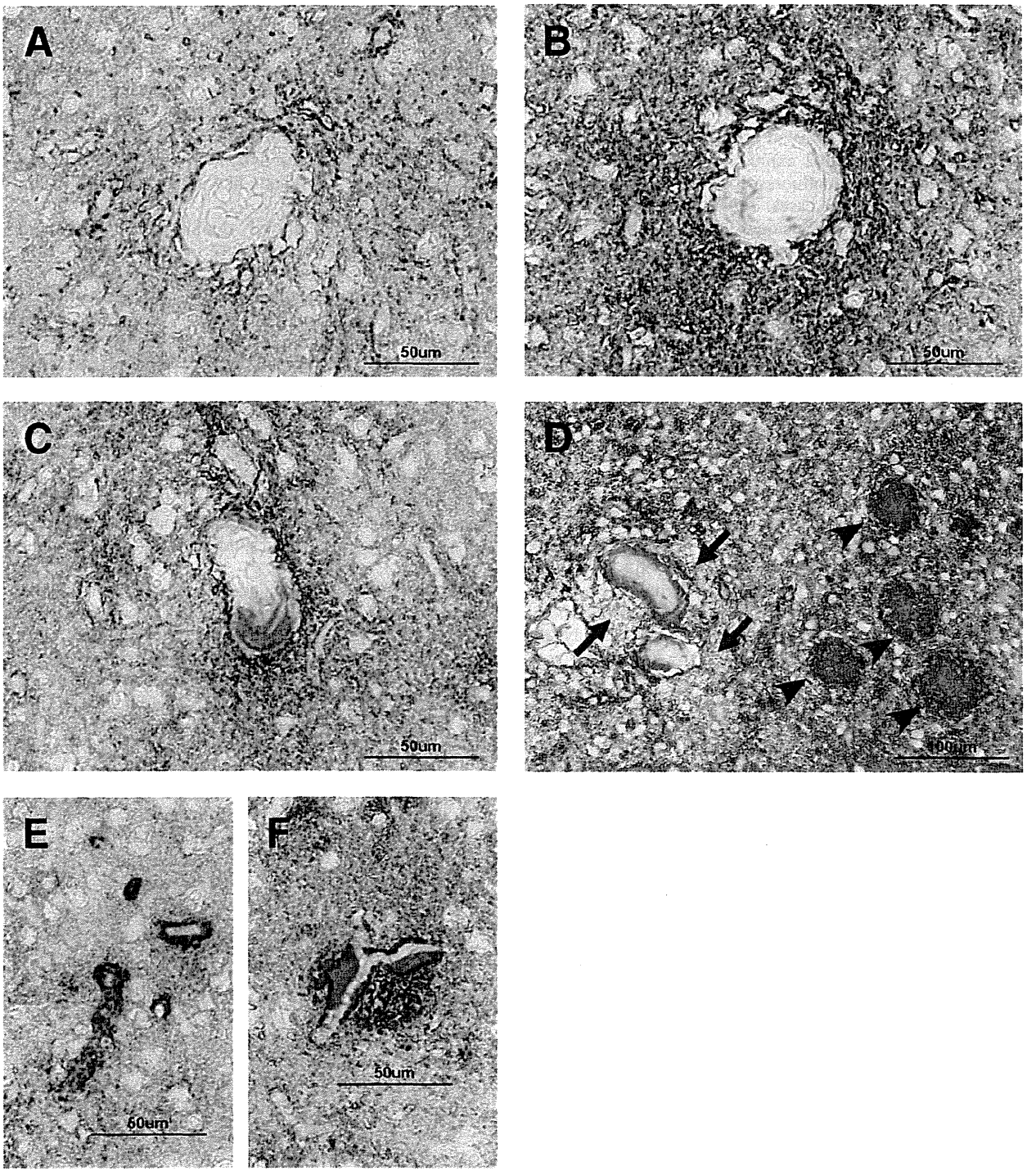

FIGURE 5. (A–F) Double-labeling immunohistochemistry for aquaporin 4 (AQP4) (brown) and amyloid β peptide 1–40 (Aβ40, red) in the Alzheimer disease (AD) groups with moderate or extensive Aβ40 deposits. Note the location of AQP4 expression around Aβ40-positive vessels. Strong AQP4 immunoreactivity is evident around slightly Aβ40-positive larger vessels **(B)** or moderately Aβ40-positive larger vessels **(C)** in comparison to the immunoreactivity around Aβ40-negative vessels **(A)**. **(D)** Loose fibrous expression of AQP4 around intensely Aβ40-positive larger vessels (arrows) and intense expression of AQP4 around areas with a high Aβ40 plaque burden (arrowheads). **(E, F)** AQP4 expression around cerebral amyloid angiopathy (CAA). Mild expression of AQP4 around capillary CAA showing slight or absent dyshoric change **(E)**. Intense expression of AQP4 around capillary CAA with dyshoric change **(F)**.

precursor protein mutation, but not a case with presenilin mutation, seemed to show more widespread Aβ plaque-like AQP4 expression than sAD cases. Because of the small number of fAD or sAD cases showing Aβ plaque-like AQP4 expression, we were unable to perform statistical analysis to clarify this issue.

Our present observations suggest that AQP1-expressing astrocytes accumulate at sites of Aβ42 or Aβ40 deposition, where they attempt to take up and degrade the Aβ (26). We consider that during the development of AD pathology, AQP1-expressing astrocytes might contribute, at least temporarily, to a reduction in local SP formation. Although the close relationship between Aβ plaques and microglial cells has been extensively studied, the role of astrocytes in Aβ plaque processing and metabolism is unclear (7, 8, 10, 27). However, it has been suggested that astrocytes have an important role in maintaining Aβ homeostasis in the AD brain. Indeed, large amounts of Aβ have been observed in activated astrocytes in human AD brain (1, 7), and some studies have shown that astrocytes can internalize Aβ both in vitro and ex vivo (6, 9, 11, 27). Furthermore, the amount of Aβ accumulated by astrocytes has been shown to correlate with the severity of AD-associated neuropathology (27), thus strengthening the view that astrocytes are key mediators of Aβ pathology. Although some studies have noted that a subpopulation of activated astrocytes express an Aβ-degrading enzyme that may play a role in Aβ clearance (6, 9, 28), the AQP1-expressing astrocytes demonstrated in the present study might also play a crucial role in SP formation.

In addition, astrocytic AQP1 expression in the AD brain seems to be important for enhancement of astrocyte migration. Cell migration generally involves the formation of membrane protrusions (lamellipodia and membrane ruffles) at the leading edge of the cell. In Chinese hamster ovary cells, exogenously expressed AQP1 is localized at lamellipodia (29), leading to the production of extensive protrusions and accelerated cell migration. Accordingly, it can be hypothesized that the expression of AQP1 observed in our AD cases might play a role in enhancing the ability of astrocytes to migrate toward Aβ plaques. This would also imply that astrocytes might lose their AQP1 expression in the presence of Aβ or other factors in areas with a dense Aβ42 burden. In other words, Aβ42-overburdened astrocytes lacking AQP1 expression might be involved in a process that will result in the formation of astrocyte-derived plaques (7, 30).

In general, although AQP1 is constitutively expressed in the choroid plexus, several studies have demonstrated that astrocytes elsewhere in the brain can express AQP1 under certain pathologic conditions, such as Creutzfeldt-Jacob disease (31), astrocytoma (22), epilepsy (32), and other processes involving astrocytic proliferation (33–36). However, it is still unclear why astrocytic AQP1 expression is upregulated in these disorders when there is no accompanying accumulation of Aβ. Using an Aβ11–25 antibody reactive with both Aβ42 and Aβ40 antigens, Misawa et al (13) have shown that the number of Aβ/AQP1–immunoreactive plaques in AD was significantly higher than in non-AD conditions such as Parkinson disease, multiple-system atrophy, amyotrophic lateral sclerosis, and some other diseases. In AD, increment of Aβ/AQP1–immunoreactive plaques may be a neuropathologic feature that distinguishes it from other neurodegenerative diseases.

Another conspicuous feature in the present study was the expression of AQP4 at SPs or around areas of CAA. Moftakhar et al (14) also studied the distribution of AQP4 plaque-like bodies in human AD brains, but they did not differentiate between Aβ42 and Aβ40 with regard to the respective association of each with AQP4 and did not describe the morphology of AQP4 plaque-like expression in detail. We found that intense Aβ plaque-like expression of AQP4 was closely associated with Aβ42 plaques and that mature SPs involving Aβ40 or dense-cored Aβ plaques lacked internal expression of AQP4. The distribution of AQP4 expression around SPs in the present study suggests that the AQP4 may play a key role in SP formation in AD. It is considered that the amyloid in the cores of classic plaques is older than that in primitive plaques and that the cores are surrounded by a halo of younger amyloid (37). Thus, the expression of AQP4 in SPs seems to occur during early Aβ deposition, whereas AQP4 downregulation seems to occur in the later stage of Aβ plaque formation.

We also noted alterations of AQP4 expression around larger vessels or capillaries affected by CAA; AQP4 expression seemed to vary depending on the severity of CAA. In general, Aβ infiltrates all layers of the vessel wall with progression of CAA, and intracortical vessels including capillaries can show additional spread of Aβ into the surrounding neuropil (so-called dyshoric change) (38, 39). In addition, many studies have shown that vascular Aβ in CAA is predominantly composed of Aβ40 (1, 4, 38), and our findings in CAA in the present series are in accord with those reports. Two studies have reported the changes in AQP4 expression associated with CAA affecting larger vessels (14, 40), and we observed some differences in the distribution of AQP4 immunoreactivity around areas of mild to moderate, or marked, Aβ40 deposition associated with dyshoric change in larger vessels or capillaries. These findings suggest that Aβ-laden blood vessels do interact with astrocytes during CAA progression. In particular, the latter pattern of AQP4 expression around areas of marked Aβ40 deposition is characterized morphologically by glial scar formation (16, 41). In the presence of dyshoric vascular Aβ deposition, clusters of activated microglia and astrocytes have been observed in perivascular areas (39), and upregulation of AQP4 in astrocytes has been found in various inflammatory lesions (42). The inflammatory reaction related to CAA with dyshoric change seems to give rise to enhancement of AQP4 immunoreactivity around areas of CAA.

In summary, we have demonstrated marked changes in the expression of AQP1 and AQP4 in relation to SPs or CAA in human brains affected by AD. Although the number of cases examined was limited, we obtained largely consistent observations that allow us to propose a model for the relationship between AQPs and Aβ. Further studies will be needed to verify the proposed mechanistic link between AQPs and the process of Aβ pathology in AD and to clarify the relationship between AQP-mediated water balance and neurodegenerative process.

ACKNOWLEDGMENT

The authors thank Junko Takasaki and Chieko Tanda for their technical assistance.

REFERENCES

1. Duyckaerts C, Delatour B, Potier MC. Classification and basic pathology of Alzheimer disease. Acta Neuropathol 2009;118:5–36
2. Iwatsubo T, Okada A, Suzuki N, et al. Visualization of Aβ42(43) and Aβ40 in senile plaques with end-specific Aβ monoclonals: Evidence that an initially deposited species is Aβ42(43). Neuron 1994;13:45–53
3. Sgourakis NG, Yan Y, McCallum SA, et al. The Alzheimer's peptides Aβ40 and 42 adopt distinct conformations in water: A combined MD/NMR study. J Mol Biol 2007;368:1448–57
4. Suzuki N, Iwatsubo T, Odaka A, et al. High tissue content of soluble β1–40 is linked to cerebral amyloid angiopathy. Am J Pathol 1994;145: 452–60
5. Mann DM, Pickering-Brown SM, Takeuchi A, et al. Amyloid angiopathy and variability in amyloid β deposition is determined by mutation position in presenilin-1–liked Alzheimer's disease. Am J Pathol 2001;158: 2165–75
6. Koistinaho M, Lin S, Wu X, et al. Apolipoprotein E promotes astrocyte colocalization and degradation of deposited amyloid-β peptides. Nat Med 2004;10:719–26
7. Nagele RG, Wegiel J, Venkataraman V, et al. Contribution of glial cells to the development of amyloid plaques in Alzheimer's disease. Neurobiol Aging 2004;25:663–74
8. Nielsen HM, Mulder SD, Beliën JA, et al. Astrocytic Aβ1–42 uptake is determined by Aβ aggregation state and the presence of amyloid-associated proteins. Glia 2010;58:1235–46
9. Wyss-Coray T, Loike JD, Brionne TC, et al. Adult mouse astrocytes degrade amyloid-β in vitro and in situ. Nat Med 2003;9:453–57
10. Mandybur TI, Chuirazzi CC. Astrocytes and the plaques of Alzheimer's disease. Neurology 1990;40:635–39
11. Verkhratsky A, Olabarria M, Noristani HN, et al. Astrocytes in Alzheimer's disease. Neurotherapeutics 2010;7:399–412
12. Huysseune S, Kienlen-Campard P, Hébert S, et al. Epigenetic control of aquaporin 1 expression by the amyloid precursor protein. FASEB J 2009; 23:4158–67
13. Misawa T, Arima K, Mizusawa H, et al. Close association of water channel AQP1 with amyloid-β deposition in Alzheimer disease brains. Acta Neuropathol 2008;116:247–60
14. Moftakhar P, Lynch MD, Pomakian JL, et al. Aquaporin expression in the brains of patients with or without cerebral amyloid angiopathy. J Neuropathol Exp Neurol 2010;69:1201–9
15. Pérez E, Barrachina M, Rodríguez A, et al. Aquaporin expression in the cerebral cortex is increased at early stages of Alzheimer disease. Brain Res 2007;1128:164–74
16. Badaut J, Ashwal S, Obenaus A. Aquaporins in cerebrovascular disease: A target for treatment of brain edema? Cerebrovasc Dis 2011;31:521–31
17. Badaut J, Lasbennes F, Magistretti PJ, et al. Aquaporins in brain: Distribution, physiology, and pathophysiology. J Cereb Blood Flow Metab 2002;22:367–78
18. Tait MJ, Saadoun S, Bell BA, et al. Water movements in the brain: Role of aquaporin. Trends Neurosci 2008;31:37–43
19. Yool AJ. Aquaporins: Multiple roles in the central nervous system. Neuroscientist 2007;13:470–85
20. Aoki K, Uchihara T, Tsuchiya K, et al. Enhanced expression of aquaporin 4 in human brain with infarction. Acta Neuropathol 2003;106:121–24
21. Hoshi A, Yamamoto T, Shimizu K, et al. Chemical preconditioning-induced reactive astrocytosis contributes to the reduction of post-ischemic edema through aquaporin-4 downregulation. Exp Neurol 2011;227:89–95
22. McCoy E, Sontheimer H. Expression and function of water channels (aquaporins) in migrating malignant astrocytes. Glia 2007;55:1034–43
23. Manley GT, Fujimura M, Ma T, et al. Aquaporin-4 deletion in mice reduces brain edema after acute water intoxication and ischemic stroke. Nat Med 2000;6:159–63
24. Braak H, Braak E. Neuropathological stageing of Alzheimer-related changes. Acta Neuropathol 1991;82:239–59
25. Hoshi A, Nakahara T, Kayama H, et al. Ischemic tolerance in chemical preconditioning: Possible role of astrocytic glutamine synthetase buffering glutamate-mediated neurotoxicity. J Neurosci Res 2006;84:130–41
26. Sofroniew MV, Vinters HV. Astrocytes: Biology and pathology. Acta Neuropathol 2010;119:7–35
27. Allamann I, Bélanger M, Magistretti PJ. Astrocyte-neuron metabolic relationships: For better and for worse. Trends Neurosci 2011;34:76–87
28. Dorfman VB, Pasquini L, Riudavets M, et al. Differential cerebral deposition of IDE and NEP in sporadic and familial Alzheimer's disease. Neurobiol Aging 2010;31:1743–57
29. Verkman AS. More than just water channels: Unexpected cellular roles of aquaporins. J Cell Sci 2005;118:3225–32
30. Nuutinen T, Huuskonen J, Suuronen T, et al. Amyloid-β 1–42 induced endocytosis and clusterin/apoJ protein accumulation in cultured human astrocytes. Neurochem Int 2007;50:540–47
31. Rodríguez A, Pérez-Gracia E, Espinosa JC, et al. Increased expression of water channel aquaporin 1 and aquaporin 4 in Creutzfeldt-Jacob disease and in bovine spongiform encephalopathy-infected bovine-PrP transgenic mice. Acta Neuropathol 2006;112:573–85
32. Zhou S, Sun X, Liu L, et al. Increased expression of aquaporin-1 in the anterior temporal neocortex of patients with intractable epilepsy. Neurol Res 2008;30:400–5
33. Hayashi Y, Edwards N, Proescholdt MA, et al. Regulation and function of aquaporin-1 in glioma cells. Neoplasia 2007;9:777–87
34. Nesic O, Lee J, Unabia GC, et al. Aquaporin 1—A novel player in spinal cord injury. J Neurochem 2008;105:628–40
35. McCoy E, Sontheimer H. MAPK induces AQP1 expression in astrocytes following injury. Glia 2010;58:209–17
36. Satoh J, Tabunoki H, Yamamura T, et al. Human astrocytes express aquaporin-1 and aquaporin-4 in vitro and in vivo. Neuropathology 2007; 27:245–56
37. Fiala JC. Mechanism of amyloid plaque pathogenesis. Acta Neuropathol 2007;114:551–71
38. Attems J. Sporadic cerebral amyloid angiopathy: Pathology, clinical implications, and possible pathomechanisms. Acta Neuropathol 2005; 110:345–59
39. Richard E, Carrano A, Hoozemans JJ, et al. Characteristics of dyshoric capillary cerebral amyloid angiopathy. J Neuropathol Exp Neurol 2010; 69:1158–67
40. Wilcock DM, Vitek MP, Colton CA. Vascular amyloid alters astrocytic water and potassium channels in mouse models and humans with Alzheimer's disease. Neuroscience 2009;159:1055–69
41. Auguste KI, Jin S, Uchida K, et al. Greatly impaired migration of implanted aquaporin-4–deficient astroglial cells in mouse brain toward a site of injury. FASEB J 2007;21:108–16
42. Aoki-Yoshino K, Uchihara T, Duyckaerts C, et al. Enhanced expression of aquaporin 4 in human brain with inflammatory diseases. Acta Neuropathol 2005;110:281–88

Parkinsonism and Related Disorders 18 (2012) 677–679

Contents lists available at SciVerse ScienceDirect

Parkinsonism and Related Disorders

journal homepage: www.elsevier.com/locate/parkreldis

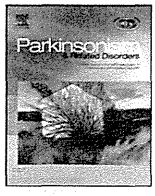

Letter to the Editor

A serial MRI study in a patient with progressive supranuclear palsy with cerebellar ataxia

Keywords:
Progressive supranuclear palsy
Cerebellar ataxia
Magnetic resonance imaging

Several clinical variants of progressive supranuclear palsy (PSP) have been identified [1]. We have recently defined a variant of patients designated PSP with cerebellar ataxia (PSP-C) [2]. Because these patients develop cerebellar ataxia as the initial and principal symptom, they might be clinically misdiagnosed as having spinocerebellar degeneration (SCD). To distinguish PSP-C from SCD, magnetic resonance imaging (MRI) [3] may be useful.

Here, we report the clinical course and serial MRI findings of a patient with pathologically proven PSP-C.

A 72-year-old Japanese man who developed unsteadiness of gait visited our hospital 1 year after its onset. Neurological examinations revealed supranuclear gaze palsy, axial rigidity, and limb and truncal ataxia. Although an initial brain MRI did not show obvious atrophy of the cerebellum (Fig. 1a–c), he was diagnosed as having SCD on the basis of clinical symptoms. Subsequently, the patient had frequent falls because of worsening of truncal ataxia. Two years after the onset, the second brain MRI was performed, which showed dilatation of pontocerebellar cistern (Fig. 1e,f) in addition to atrophy of the superior cerebellar peduncles (SCPs) (Fig. 1e). The third brain MRI, performed 4 years after the onset, showed the increased dilatation of pontocerebellar cistern, proportional but "small in size" pons and cerebellum with fourth ventricular dilatation (Fig. 1i), and the rostral midbrain atrophy (Fig. 1g). The progressive dilation of pontocerebellar cistern was confirmed by quantitative analyses: the area of pontocerebellar cistern at the level of middle cerebellar peduncles on the initial, second, and third MRIs are 7.5 mm^2 (12.6% of posterior fossa), 13.7 mm^2 (20.0% of posterior fossa), and 17.4 mm^2 (29.9% of posterior fossa), respectively (Fig. 1c,f,i). The progressive rostal midbrain atrophy was also confirmed [3]: the area of tegmentum mesencephali on the initial, second, and third MRIs are 103.8 mm^2, 69.2 mm^2, and 47.1 mm^2, respectively (Fig. 1a,d,g). At 76-year-old, he died from CO_2 narcosis. The diagnosis of PSP was confirmed after autopsy [2]. Briefly, tau-positive inclusion bodies in Purkinje cells (Fig. 2) and severe neuronal loss with gliosis in the dentate nucleus were observed.

We provide, for the first time, serial MRI findings in a pathologically proven PSP-C patient. When the patient developed cerebellar ataxia as an initial symptom, MRI did not show obvious atrophy of the cerebellum. However, follow-up MRI examinations demonstrated atrophy of the SCPs as well as dilatation of pontocerebellar cistern that accompanies "small in size" pons and cerebellum. The former finding has been shown on volumetric MR images in patients with PSP [3]. On the other hand, the latter finding was previously reported in a pathologically proven PSP patients who developed cerebellar ataxia as the initial and principal symptom: CT scans of the patient revealed no obvious atrophy of cerebellum in early-stage of the disease and enlarged pontocerebllar cistern in advanced-stage of the disease [4]. We consider that dilatation of pontocerebellar cistern that accompanies "small in size" pons and cerebellum might be characteristic imaging feature of PSP-C.

This patient is of interest to understand lesions responsible for ataxia in PSP patients. On the basis of our pathological examination of patients with PSP-C, we speculated that patients with tau-positive inclusion bodies in Purkinje cells and degenerated dentate nucleus easily develop cerebellar ataxia [2]. This speculation might be supported by a recent clinicopathological analysis of 30 Caucasian PSP patients, which demonstrated that cerebellar ataxia was exclusively observed in 2 patients who exhibited tau-positive inclusion bodies in Purkinje cells [5]. Future studies need to be performed to understand the mechanism by which cerebellum and pons become atrophic proportionally in PSP-C patients.

In conclusion, this case report suggest that dilatation of pontocerebellar cistern that accompanies "small in size" pons and cerebellum might be characteristic imaging feature of PSP-C, although accumulation of patients and analyses will be necessary.

1353-8020/$ – see front matter
doi:10.1016/j.parkreldis.2011.11.011

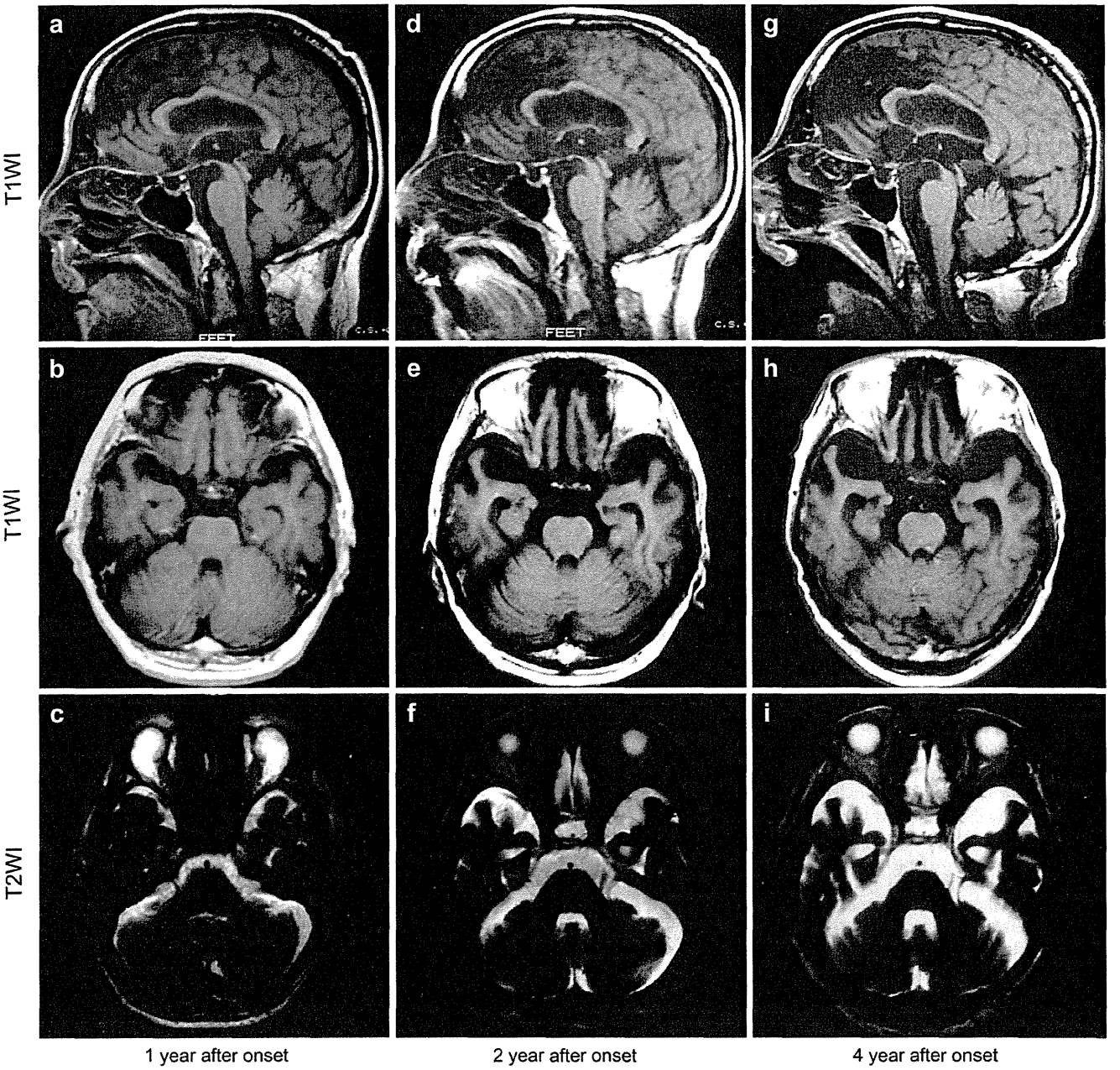

Fig. 1. A serial MRI study in the present patient. Top panels (a, d, g), sagittal T1-weighted MRIs (T1WIs) at the level of the mesencephalic aqueduct. Middle panels (b, e, h), axial T1WIs at the level of the superior cerebellar peduncles. Lower panels (c, f, i), axial T2-weighted MRIs (T2WIs) at the level of the middle cerebellar peduncles. Serial MRIs showed atrophies of the midbrain (g), superior cerebellar peduncles (e, h), and frontal and temporal lobes (e, h), in addition to enlarged pontocerebellar cistern without overt dilatation of cerebellar fissures (i).

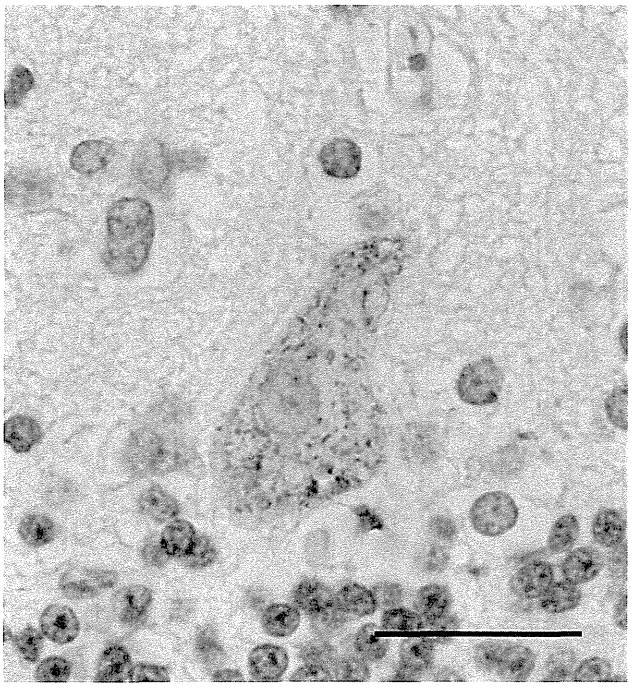

Fig. 2. Immunohistochemical finding of Purkinje cells. High-power magnifications view of a Purkinje cell demonstrating granular, tau-positive profiles in the cytoplasm by AT8 immunostain. Bar = 25 μm.

Disclosure

The authors report no conflicts of interest.

References

[1] Williams DR, Lees AJ. Progressive supranuclear palsy: clinicopathological concepts and diagnostic challenges. Lancet Neurol 2009;8:270–9.
[2] Kanazawa M, Shimohata T, Toyoshima Y, Tada M, Kakita A, Morita T, et al. Cerebellar involvement in progressive supranuclear palsy: a clinicopathological study. Mov Disord 2009;24:1312–8.
[3] Stamelou M, Knake S, Oertel WH, Hoglinger GU. Magnetic resonance imaging in progressive supranuclear palsy. J Neurol 2011;258:549–58.
[4] Aiba I, Saito Y, Yasuda T, Yoshida M, Hashizume Y. Progressive supranuclear palsy with cerebellar ataxia. An autopsy case. Shinkeinaika 2002;56:230–3 [in Japanese].
[5] Jellinger K. Cerebellar involvement in progressive supranuclear palsy. Mov Disord 2010;25:1104–5.

Masato Kanazawa, Takayoshi Shimohata*
Department of Neurology, Brain Research Institute, Niigata University, 1-757 Asahimachi-dori, Chuoku, Niigata, Niigata 951-8585, Japan

Kotaro Endo, Ryoko Koike
Department of Neurology, Nishi-Niigata Chuo National Hospital, Niigata, Japan

Hitoshi Takahashi
Department of Pathology, Brain Research Institute, Niigata University, Niigata, Japan

Masatoyo Nishizawa
Department of Neurology, Brain Research Institute, Niigata University, 1-757 Asahimachi-dori, Chuoku, Niigata, Niigata 951-8585, Japan

* Corresponding author. Tel.: +81 25 227 0666; fax: +81 25 223 6646.
E-mail address: t-shimo@bri.niigata-u.ac.jp (T. Shimohata)

30 September 2011